ACS Photonics

Article

pubs.acs.org/journal/apchd5

Controlling Electric and Magnetic Resonances for Ultracompact Nanoantennas with Tunable Directionality

Kan Yao[†] and Yongmin Liu*[,†,‡]

[†]Department of Electrical and Computer Engineering and [‡]Department of Mechanical and Industrial Engineering, Northeastern University, Boston, Massachusetts 02115, United States

Supporting Information

ABSTRACT: We design and numerically demonstrate an ultracompact plasmonic nanoantenna with tunable high directionality. The antenna consists of a metallic trimer that can support a highly spectrally tunable magnetic dipole mode with its amplitude comparable to that of an electric dipole mode. Superior forward radiation is achieved when these modes satisfy the Kerker conditions, leading to a very low side lobe level of −22 dB. It is shown that by moving one of the three particles by less than 10 nm the resonance wavelength of the magnetic mode will shift dramatically, resulting in the change of the interference conditions and hence the radiation characteristics. From the evolution of the resonant modes, we find optimized designs that reverse the radiation direction at the same wavelength. Meanwhile, the enhancement of spontaneous emission and radiated power of a nanoemitter adjacent to the antenna can reach approximately 4 and 3 orders of magnitude, respectively. Analyses based on a simple dipole model are performed, and the reconstructed radiation patterns agree well with the simulation results.

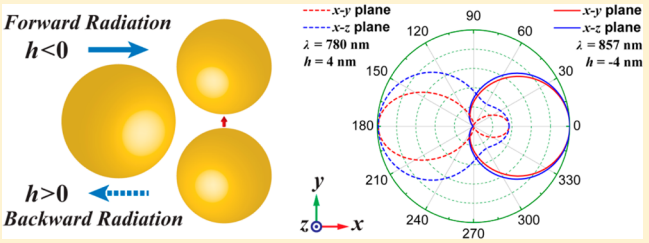

KEYWORDS: *nanoantennas, metallic nanoparticles, magnetic dipole, radiation control, Purcell effect*

Nanoantennas, the counterparts of radiowave and microwave antennas at optical frequencies, are able to efficiently couple the energy of free-space radiation to a confined region of subwavelength dimensions or vice versa. They have been used in a broad range of nano-optical applications, including near-field microscopy,[1,2] spectroscopy,[3] and photovoltaics.[4] Nanoantennas are also considered a promising candidate for single-photon sources[5] and nonlinearity enhancement.[6,7] Among various designs, unidirectional nanoantennas have attracted particular interest.[8−16] From the practical point of view, a nanoantenna with unidirectional radiation and reception properties can facilitate the excitation and detection of nanoemitters, such as fluorescence molecules or quantum dots (QDs), which usually have very small absorption and scattering cross-section due to the large mismatch between the wavelengths and the size of the nanoemitters. In order to efficiently direct light emission in a certain direction, one strategy is to scale down the dimensions of the classical radiowave or microwave antenna designs. For example, the investigation of optical Yagi−Uda antennas has achieved remarkable success,[9,16−19] in which the directionality relies on the coupling of electric dipoles (EDs) with proper relative phase induced in each element. However, the separation of the elements is about a quarter-wavelength.[17] This implies the entire array can hardly be ultracompact in size, hindering the further miniaturization of optical antennas.

Higher order resonances of nanostructures provide additional degrees of freedom to engineer the emission or scattering characteristics, which enable directional control of light propagation by compact nanostructures. It has been recently demonstrated that the electric dipole−quadrupole interference plays a dominant role in directional light emission from QDs coupled to a split ring resonator (SRR)[14,20] and from fluorescence molecules coupled to a V-shaped nanoantenna.[15] A similar strategy to control directional scattering has been reported for metallic spheres[21] and V-shaped nanorods.[22] Utilization of magnetic responses has been explored as well. A high-index dielectric or core−shell nanoparticle that supports a magnetic dipole (MD) mode spectrally overlapping with the ED mode shows directional scattering in the visible and near-infrared regime.[23−26] When an emitter is coupled to a high-index particle under restricted conditions, a magnetic quadrupole can be induced to obtain improved radiation directivity.[27] However, the use of dielectrics sacrifices the enhancement of spontaneous emission.[28] Simultaneous control of the emission directionality and radiation enhancement requires an innovative design based on noble metals. Nevertheless, in most metallic nanostructures, the magnetic resonances are too weak to be effectively utilized. So far, only a few structures, for example, SRRs and closely packed nanoparticle clusters, have been proven to exhibit significant contribution from the MD in the scattering spectra.[29−32] Furthermore, conventional nanostructures have fixed geometry after fabrication, and therefore their tunability is very limited. Adjusting the radiation or scattering

Received: December 7, 2015
Published: May 24, 2016

DOI: 10.1021/acsphotonics.5b00697
ACS Photonics 2016, 3, 953−963

properties, if possible, can be achieved only at different wavelengths.

In this article, we numerically study an ultracompact plasmonic nanoantenna with tunable high directionality and its interaction with nanoemitters. The antenna, consisting of a nanoparticle trimer, can support a strong and highly tunable MD mode that spectrally overlaps the ED mode. Such tunability arises from the nanoscale control over the interparticle distance of the trimer, which potentially can be realized by DNA-regulated conformational changes. It is demonstrated that the interference between the magnetic and electric dipole modes gives rise to superior unidirectional radiation from a nanoemitter coupled to the nanoantenna. The side lobe level, when the Kerker conditions are well satisfied, can be suppressed down to −22 dB in the case of forward radiation. By tracking the evolution of the resonant modes, we show that the resonance wavelength of the MD will shift dramatically when one particle is displaced by less than 10 nm, strongly modifying the interference conditions and hence the radiation characteristics. With proper arrangements of the particles, the majority of the emitted photons can be steered in the opposite direction. The designs are further optimized so that the reverse of directionality can be achieved at the same wavelength. Both forward and backward radiations are analyzed using a simple dipole model, and the reconstructed radiation patterns are in good agreement with simulation results. The resonant plasmonic modes also render remarkable emission enhancement. Quantitative calculation reveals that the spontaneous emission rate and the radiated power are enhanced respectively by about 4 and 3 orders of magnitude, promising an ultrafast, ultrabright, and ultracompact light source with excellent and tunable directionality.

Figure 1 shows the schematic of the nanoantenna. The device comprises three gold nanoparticles arranged into an asymmetric trimer configuration. Nanoparticle clusters have aroused increasing attention for their sophisticated, hybridized plasmon modes[32−34] and their potential applications for optical metamaterials.[30,35] In particular, the impact of symmetry in identical spheres has been studied,[31,36,37] while to date the understanding and knowledge on asymmetric clusters are still largely unexplored.[38] Here, we break the structural symmetry into two aspects. First, the sizes of the particles are not identical: Two of them have a diameter D_1 = 100 nm, and the third one has D_2 = 120 nm, providing different polarizabilities in response to the excitation. Second, the interparticle spacing is not identical either. The two smaller particles form a dimer lying along the y-axis, which are separated by a distance g_1 of 5 nm with a nanoemitter positioned at the center. The larger particle, which holds equal distances g_2 from the two smaller ones, can be moved along the x-axis slightly toward or away from the dimer, resulting in different interparticle coupling strengths that can modify the radiation properties. To clearly describe the change of the configuration, we define an equilibrium position for the larger particle as a reference, where the three particles are all separated from each other by 5 nm ($g_2 = g_1$). Relative to this position, translating the larger particle toward (away from) the dimer corresponds to negative (positive) displacement h. In the simulations based on the finite integration technique (CST Microwave Studio) and the finite element method (COMSOL Multiphysics), the nanoemitter is modeled as an ED. When the emitter is oriented along the y-axis, it is coupled most efficiently to the plasmonic resonance of the two adjacent smaller particles, while other orientations are also studied for practical reasons. The permittivity of gold is taken from the Johnson and Christy data,[39] and the background medium is assumed to be an aqueous solution (refractive index n = 1.33). Such a configuration mimics the environment for sensing applications and is compatible with a DNA-based reconfigurable technique that allows actively altering the cluster configuration.[40−42] More details about the simulations can be found in the Methods section.

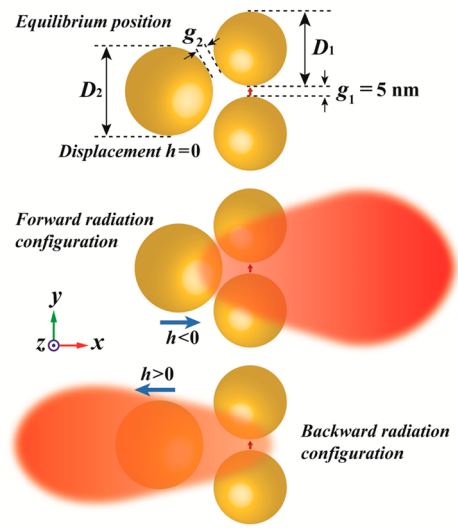

Figure 1. Schematic of the nanoantenna consisting of a plasmonic trimer with broken symmetry. The third particle (diameter D_2 = 120 nm) and those composing the dimer (diameter D_1 = 100 nm) are slightly different in size, forming an isosceles triangle. An electric dipole (ED) emitter is positioned at the center of the dimer and is oriented parallel to the gap along the y-axis. The size of the dimer gap is fixed to be g_1 = 5 nm, while the larger particle can be displaced along the x-axis. The displacement h is counted relative to the equilibrium position (top panel), where the monomer−dimer gaps (g_2) are also 5 nm. When moving the larger particle closer to the dimer (h < 0, middle panel), the radiated beam is steered toward the +x, or forward, direction, whereas when the larger particle is shifted away from the dimer (h > 0, bottom panel), the orientation of the beam is reversed to the −x, or backward, direction. Blue arrows indicate the displacement of the larger particle with respect to the equilibrium position.

In the first case, the larger particle is shifted 4 nm toward the dimer (h = −4 nm). Consequently, the gaps between the larger particle and smaller particles narrow to g_2 = 1.5 nm. This closely packed configuration gives rise to stronger interparticle coupling, from which pronounced local resonance across the gap is produced. In Figure 2a, the green curve shows the radiation spectrum characterizing the overall power P_r radiated into the far-field. Three distinct peaks are observed at 820, 715, and 595 nm. (The wavelength is defined as the wavelength in a vacuum throughout this paper.) Without employing the mode hybridization theory,[43] the origins of these peaks can be identified by probing the far-field in certain directions.[31] This simple approach avoids retrieving in a more rigorous manner the polarizability of the structure for multipole expansion,[44] but is effective in the context of ED/MD decomposition. Briefly, as the antenna is fed by a nanoemitter oriented along the y-axis in the dimer gap, a strong collective oscillation of electrons will be excited in the dimer, acting as an ED lying along the y-axis. Meanwhile, the third, larger particle is involved through interparticle coupling, which induces a current flow circulating along the nanoparticle loop. Consequently, an equivalent MD

DOI: 10.1021/acsphotonics.5b00697
ACS Photonics 2016, 3, 953−963

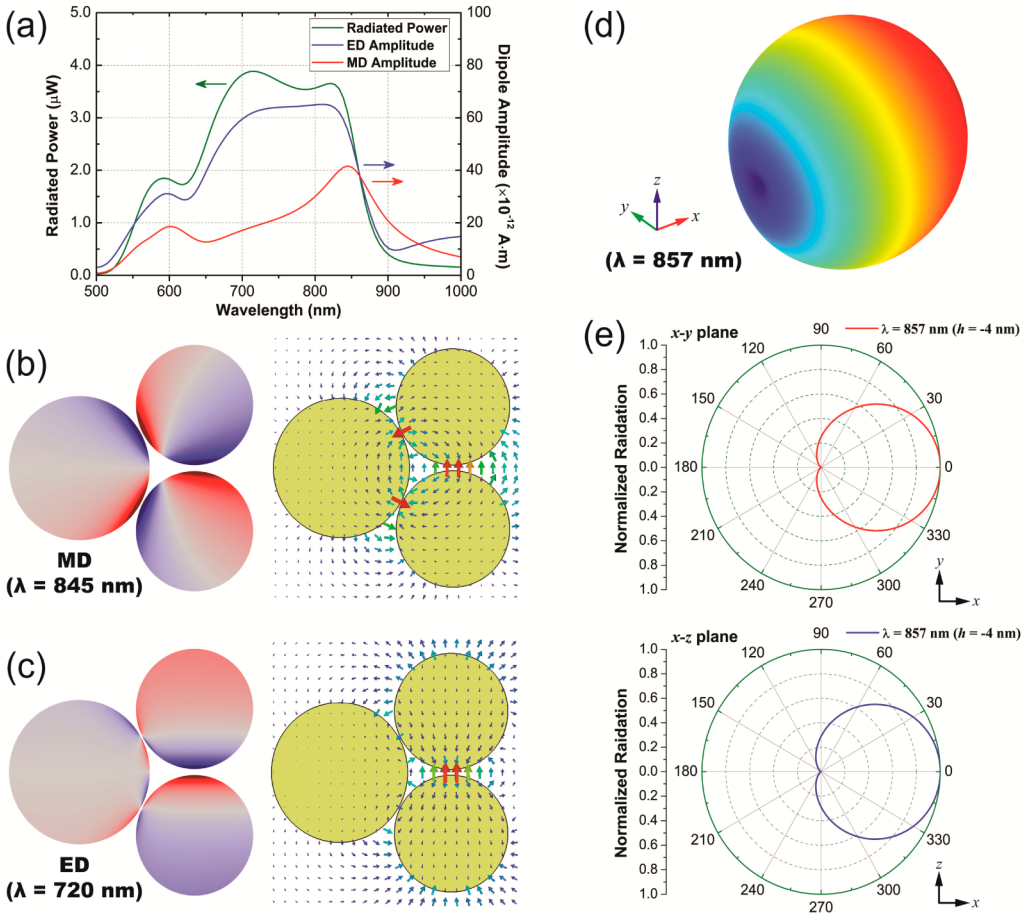

Figure 2. Simulation results for the forward-radiation configuration. The larger particle is moved 4 nm toward (+x direction, h = −4 nm) the dimer from the equilibrium position. (a) Spectra of the total radiated power (green) and of the ED (blue) and MD (red) amplitude, respectively. (b, c) Surface charge density (left panel) and electric field distribution in vector format (right panel) at (b) 845 nm and (c) 720 nm wavelengths, where the magnetic and electric resonances take place, respectively. The minimum side lobe level of −22 dB for forward radiation is observed at 857 nm, where the ED and MD have approximately equal amplitude and are nearly in phase. The near-field plots at 857 nm are very similar to those in (b), with the strength of all the field quantities decreased slightly. Corresponding plots in (b) and (c) are based on the same color scale for clarity. (d) 3D and (e) 2D radiation patterns at 857 nm.

parallel to the z-axis arises. From the radiation pattern of individual ED and MD,[14] we can readily find that the far-field emission in the x direction is the result of interference between the fields radiated by the ED and MD, and the emission in the y and z direction contains exclusively the fields from the MD and from the ED, respectively. Therefore, two probes are set in the far-field on the y- and z-axis to record the radiated fields from each dipole mode, which are then converted into the dipole amplitude based on classical formulas.[45] We would like to emphasize that the dipoles retrieved with this approach are approximations based on their far-field radiation properties. Compared with the quasi-normal solutions solved from Maxwell's equations for a system with finite dimensions with respect to the wavelength, they are "dipole-like" modes rather than the strict eigenmodes.[46,47] For conciseness reasons and without causing confusion, we still keep the terminology ED and MD throughout this paper in a similar way to some previous work.[31] Due to the symmetry and radiation properties of the electric and magnetic dipoles, the magnetic dipole amplitude is multiplied by the wavenumber k to make it consistent in dimension with the electric current dipole moment. The separated dipoles are indicated in Figure 2a by the red and blue curves. One can see that the MD mode (red curve) exhibits a Lorentzian line shape centered at 845 nm, implying a major contribution to the radiated power maximum on the long-wavelength side around 820 nm. The spectrum of the ED amplitude (blue curve), however, shows a rather broad peak ranging from 680 to 815 nm, which seems to conflict with a typical resonance feature. In fact, the curve records the emission from two origins. Because the cluster has a broken symmetry, near the magnetic resonance wavelength there is a net ED moment coexisting with the MD.[31] This net ED interacts with the intrinsic ED resonance of the dimer centered at about 720 nm, producing the broad peak as observed. The total radiated power, which contains the contributions from both the ED and MD modes, shows two maxima at 820 and 715 nm and retains high amplitude within this spectral range. For all spectra in Figure 2a, there is a third peak with weaker amplitude emerging at 595 nm. This peak originates from the higher order mode of the dimer and its complex interaction with the larger particle (see Supporting Information). Hereafter we will focus only on the ED and MD modes at wavelengths above 600 nm.

The identification of the electric and magnetic resonances is further checked in the near-field region. In Figure 2b and c, the snapshots of the surface charge density (left panel) and electric

DOI: 10.1021/acsphotonics.5b00697
ACS Photonics 2016, 3, 953−963

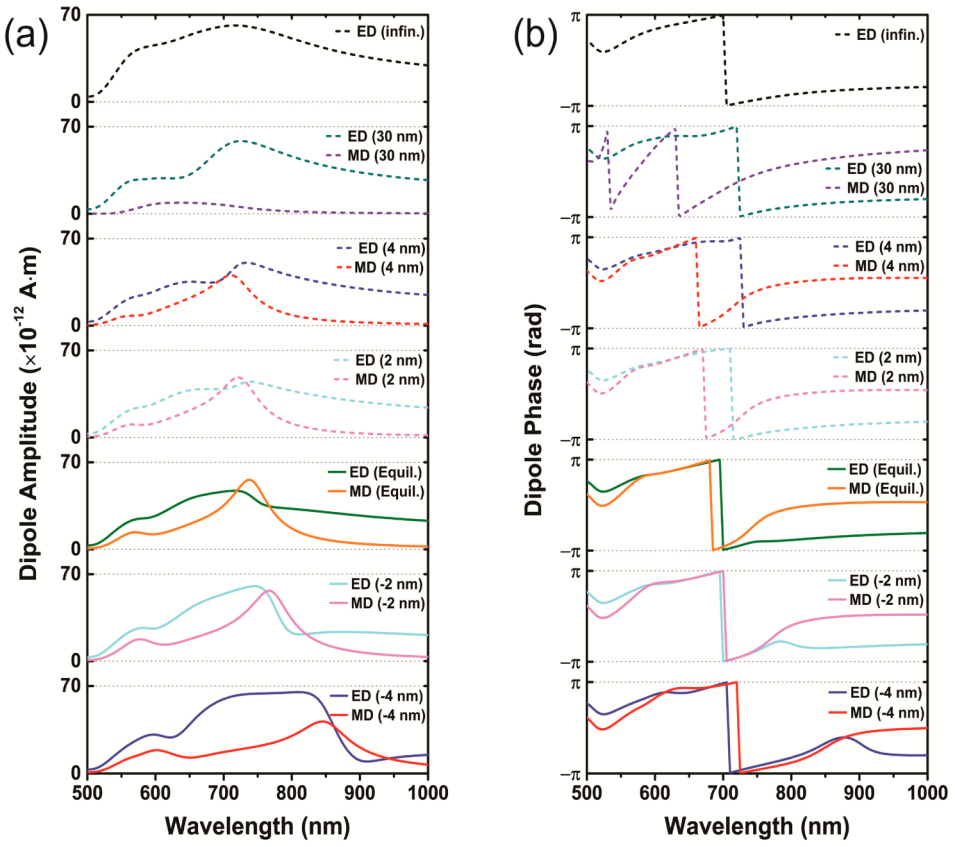

Figure 3. Evolution of the amplitude (a) and phase (b) of the dipole modes. The numbers in the legend denote the displacement h of the larger particle.

field distribution in vector format (right panel) are presented at the MD and ED resonance wavelengths, respectively. It can be clearly seen that a current loop, the unique fingerprint of a MD mode, and extremely strong local fields within the narrower gaps occur at 845 nm. As the wavelength decreases to 720 nm, these hot spots migrate to the wider gap of the dimer, showing evidently the existence of a dominant ED mode.

In Figure 2a, another noticeable characteristic is that the spectrum of the MD intersects with the spectrum of the ED at about 860 nm. From classical electromagnetic theory, a pair of ED and MD with perpendicular orientation and equal amplitude will emit light in merely one direction if the dipoles are in phase or in antiphase (i.e., with a π-phase difference). A famous paradigm based on this concept is known as Kerker scattering.[23,25,48] When the amplitude and phase deviate from the aforementioned rigorous conditions to a moderate extent, the radiation pattern can still exhibit remarkable directionality. Figure 2d and e show the simulated radiation patterns at 857 nm. It is seen from the three-dimensional (3D) contour that the majority of the radiated power is steered toward the dimer side (along the positive x-axis, defined as the forward direction), as though the larger particle functions as a reflector. The 2D patterns in Figure 2e on two perpendicular planes clearly confirm the ED−MD interference, because the radiation pattern contains only one broad main lobe while all the side lobes are eliminated.[14,26] The side lobe level, defined as the ratio of the power density in the largest side lobe (here the back lobe) to that of the main lobe, reaches an extremely small value of −22 dB. This performance is already comparable to some radiowave and microwave antennas.[49] Moreover, the side lobe level can be maintained below −10 dB from 825 to 875 nm, showing a reasonably good bandwidth.

It has been demonstrated that the magnetic resonance in the trimer structure is highly tunable.[31,33] A slight geometric modification will cause a significant shift of the resonance frequency. In order to obtain a quantitative idea on the tunability of the resonances, we track the evolution of the MD and ED spectra based upon different trimer configurations, where the larger particle is shifted along the x-axis for different values of displacement h. Figure 3a shows the simulated results. At the bottom, we illustrate again the dipole magnitude spectra for the forward radiation case, which correspond to the geometry (h = −4 nm) discussed previously in Figure 2. In the upper panels, where the larger particle is moved outward stepwise, the MD exhibits blue-shifts accordingly. The shift is significant when the particles are close to each other, while it gradually fades out as the larger particle moves far away. The magnitude of the MD resonance also shows strong dependence on the interparticle spacing. Intuitively, one may expect the maximum MD to occur when the large particle is in very close proximity to the smaller particles. However, it is revealed here that the strongest MD appears around the equilibrium configuration. For smaller gaps, the stronger local fields result in more energy dissipated into heat. The ED spectra evolve in a more complex manner. The intrinsic ED of the dimer, peaked around 720 nm, does not change much among all the configurations, whereas the induced net ED, as discussed earlier, blue-shifts with the MD resonance when the larger particle is moved outward. Depending on their relative phase, the interaction of these two modes leads to very different line

DOI: 10.1021/acsphotonics.5b00697
ACS Photonics 2016, 3, 953−963

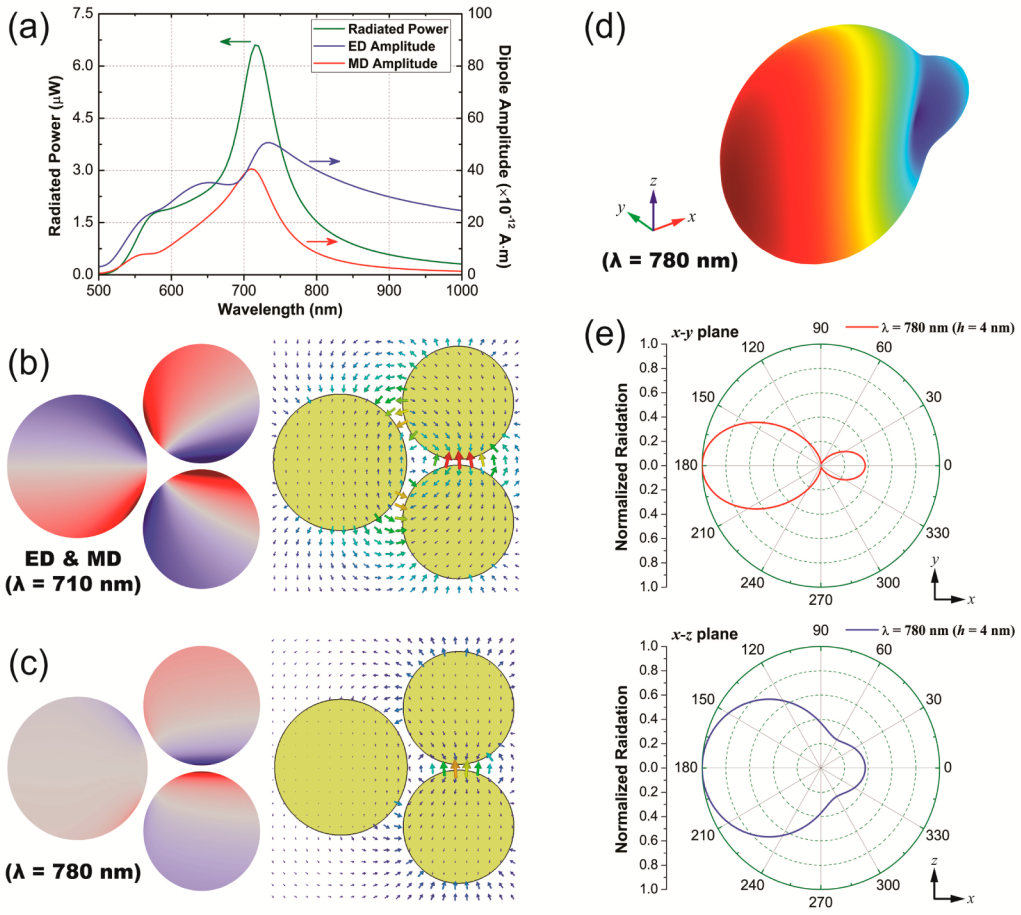

Figure 4. Simulation results for the backward-radiation configuration. The larger particle is moved 4 nm away (−x direction) from the dimer counting from the equilibrium position. (a) Spectra of the radiated power (green) and of the ED (blue) and MD (red) amplitude, respectively. (b) Surface charge density (left) and electric field distribution (right) at 710 nm, where the ED and MD modes are both on resonance. (c) Same as (b) but at 780 nm, where the minimum side lobe level of −4.2 dB for backward radiation is achieved. With larger gaps between the third particle and the dimer, the ED exhibits much stronger amplitude than the MD, as shown in both (b) and (c). (d) 3D and (e) 2D radiation patterns at 780 nm.

shapes. Probing the electric field in the far-field region also enables extraction of the phase information on the dipoles, as shown in Figure 3b. With the full knowledge of the resonant modes, it becomes possible to design nanoantennas with desirable performance.

In the following, we consider a different configuration obtained by moving the larger particle outward from the equilibrium position for 4 nm (h = 4 nm). As a result, the gap between the larger particle and two smaller particles is increased to g_2 = 8.5 nm. Similar to Figure 2a, Figure 4a shows the spectra of the total radiated power and of the ED and MD amplitude. Compared with the first case, the significant blue-shift of the MD causes better spectral overlap with the ED and thus a pronounced peak of the radiated power around 720 nm. The surface charge density and electric field distribution in Figure 4b also signify that the ED and MD are both on resonance at this wavelength with comparable amplitude. However, from Figure 3b it is noted that the phase difference is quite large, deviating far away from the ideal Kerker conditions. Therefore, one cannot achieve highly directional radiation with the maximum radiated power near 720 nm. In spite of the decreased directionality, interestingly, the main lobe can switch its orientation within a certain wavelength range, pointing toward the larger particle (along the negative x-axis, defined as the backward direction) as if it behaves as a director. Figure 4d and e plot such backward-radiation patterns at 780 nm in 3D and 2D formats, respectively, with the lowest side lobe level of about −4.2 dB. Compared with Figure 2d and e, the change of radiation patterns reflects the fact that the MD can only partially compensate the emission of the ED in the opposite direction, rendering a finite back lobe. This result is consistent with the near-field patterns in Figure 4c, where the strong local field can be evidenced only in the gap between the smaller particles, indicating a dominant ED mode and a relatively weak MD mode. The best achievable directionality from different trimer configurations can be found in the Supporting Information.

In order to demonstrate the origin of the directionality more clearly, the radiation patterns are reconstructed using a simple ED−MD interference model. Similar approaches have been adopted before to interpret the directional propagation of surface waves from the scattering of single subwavelength holes[50] and from designer sources.[51,52] For this purpose, each resonant mode is treated as a point dipole. Specifically, the ED is located at the center of the two smaller particles and oriented along the y-axis, while the MD is positioned at the centroid of the trimer and polarized along the z-axis. The amplitude and phase of each individual dipole can be precisely determined by probing the far-field, as described earlier. Therefore, by taking the vectorial summation of the fields

DOI: 10.1021/acsphotonics.5b00697
ACS Photonics 2016, 3, 953−963

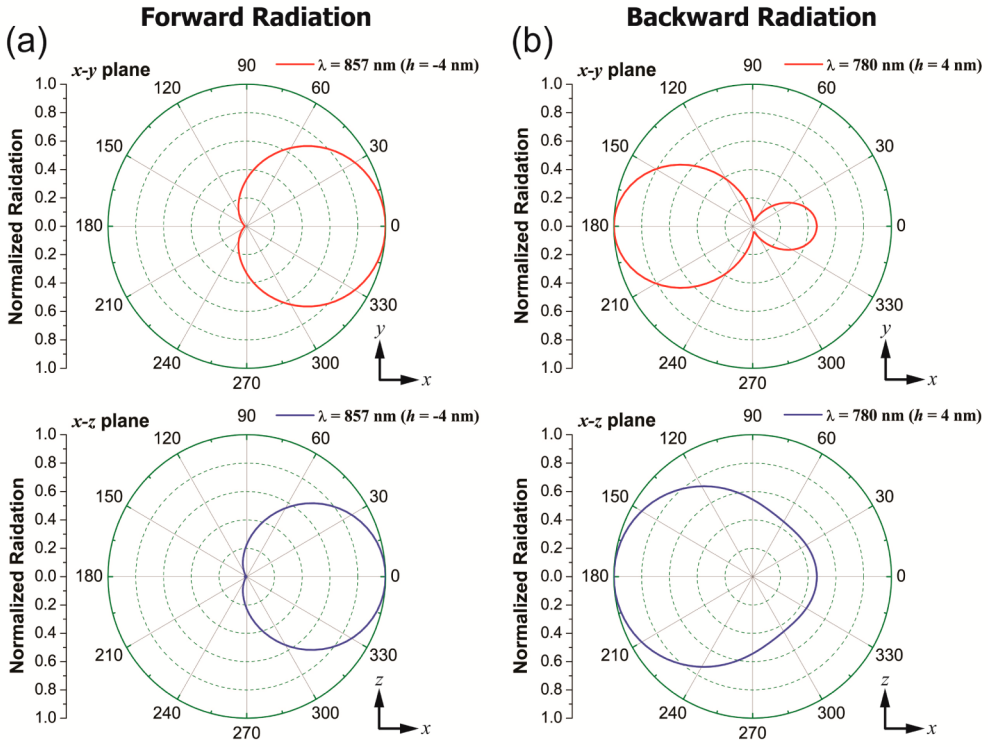

Figure 5. Radiation patterns reconstructed using the ED−MD interference model. (a) Forward radiation at 857 nm (left column, cf. Figure 2e). (b) Backward radiation at 780 nm (right column, cf. Figure 4e).

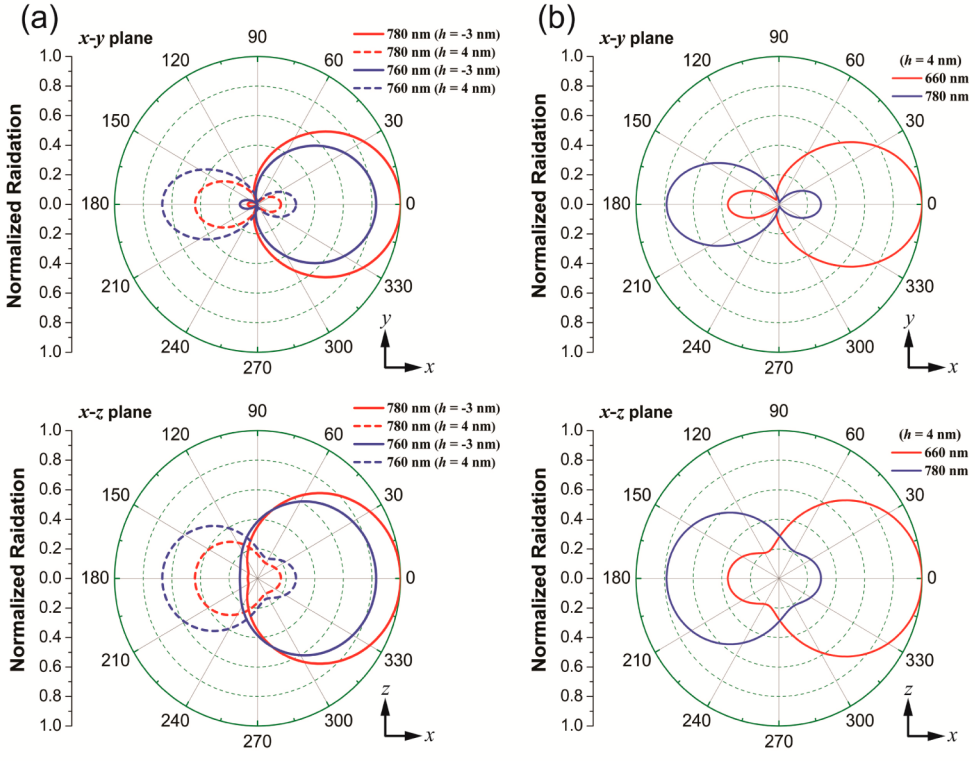

Figure 6. Reversal of radiation direction. (a) Flipping the radiation direction at the same wavelength using a reconfigurable nanoantenna (left panels). The forward radiation (solid curves) is obtained from the trimer with $h = -3$ nm, while the backward radiation (dashed curves) is from the trimer with $h = 4$ nm. Although the best directionality occurs at 780 nm, detuning the wavelength to 760 nm only slightly affects the performance, suggesting a considerably broad bandwidth. (b) Directional color routing based upon the backward-radiation configuration (right panels) with $h = 4$ nm. The main lobe is steered to opposite directions at 660 and 780 nm wavelengths.

DOI: 10.1021/acsphotonics.5b00697
ACS Photonics 2016, 3, 953−963

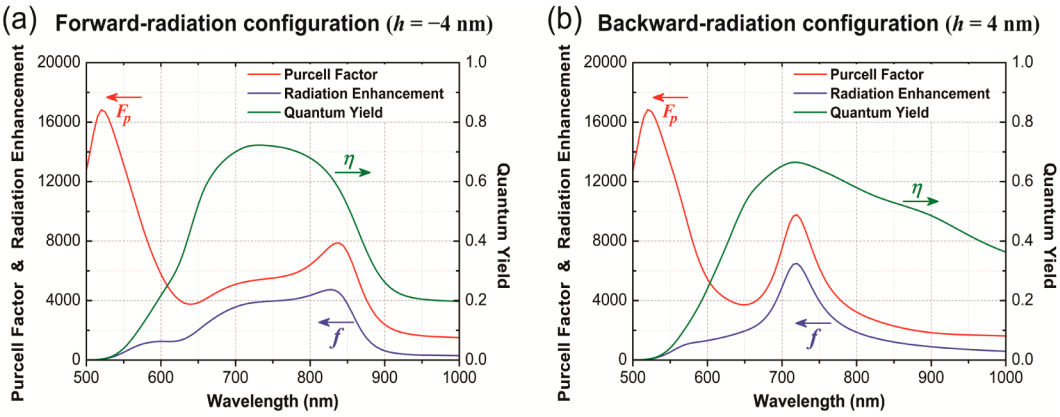

Figure 7. Spectra of the Purcell factor F_p (red), emission enhancement f (blue), and quantum yield η (green) for (a) forward-radiation configuration when $h = -4$ nm and (b) backward-radiation configuration when $h = 4$ nm, respectively.

$$\vec{E} = \frac{k^2}{4\pi\varepsilon r} e^{ikr}[(\hat{r} \times \vec{p}) \times \hat{r}] \tag{1a}$$

$$\vec{H} = \frac{ck^2}{4\pi r} e^{ikr}(\hat{r} \times \vec{p}) \tag{1b}$$

from the ED $\vec{p}$ and

$$\vec{E} = -\frac{Z \cdot k^2}{4\pi r} e^{ikr}(\hat{r} \times \vec{m}) \tag{2a}$$

$$\vec{H} = \frac{k^2}{4\pi r} e^{ikr}[(\hat{r} \times \vec{m}) \times \hat{r}] \tag{2b}$$

from the MD $\vec{m}$, the radial component of the Poynting vector can be calculated accordingly. Here ε represents the permittivity of water; k, c, and Z denote the wavenumber, speed of light, and wave impedance in water, respectively. The position of a point in the far-field is characterized by its radial distance r from the origin and the unit vector $\hat{r}$ along the radius. Figure 5a (left column) shows the 2D radiation patterns of the antenna in the forward-radiation case at 857 nm. With nearly equal amplitudes and a small deviation of phase (0.079π) determined in the earlier procedure (Figure 3), the involved ED and MD interfere in such a manner that the Kerker conditions are fairly satisfied. Compared to the patterns in Figure 2e, the number, orientation, shape, and even the ratio of the lobes are nicely reproduced. The excellent agreement between simulation and analysis based on the simple dipole model provides solid evidence for the ED−MD interpretation of the forward radiation.

As a comparison, the patterns of the backward radiation are presented in Figure 5b (right column). At 780 nm, the ED is about 3.6 times greater than the MD in amplitude and meanwhile holds a 0.761π delay in phase. Here, while the number, orientation, and shape of the lobes are reproduced correctly, the ratio of the main lobe to the back lobe shows a decrease compared with the results in Figure 4e. This deviation can be attributed to the simplification of the dipole model. Indeed, in the trimer structure, the ED and MD are the dominant resonant modes, implying that ED−MD interference is a good approximation that can capture the correct trend of the radiation pattern. Nevertheless, as the larger sphere is shifted away from the dimer in the backward-radiation configuration, the interparticle coupling becomes weaker and the electron oscillation in the larger sphere tends to have a larger component along the y-axis acting like an ED. This induced ED, together with other higher order resonant modes (e.g., electric quadrupole associated with the MD[53,54]) providing additional contribution to the radiation patterns, needs to be taken into account in the interference model. Eventually, the MD vanishes when the larger particle is separated far enough, and the physical picture of the directional emission then evolves into the model based on ED−ED interference.[11,55]

From Figure 3a, it is seen that the dipole amplitude evolves continuously with gradually changing trimer configuration. Noting that the intersection of ED and MD spectra satisfying Kerker conditions takes place at 760 and 860 nm for the $h = -2$ and -4 nm cases, respectively, we expect intermediate displacement values could lead to superior forward radiation at wavelengths in between. This spectral tunability offers opportunities to reverse the radiation direction without changing the operating wavelength. Figure 6a compares the radiation patterns for configurations with $h = -3$ and 4 nm, respectively. It is observed that the main lobe of the radiation pattern flips to the opposite direction at 780 nm wavelength, although the forward radiation shows larger amplitude and better directionality. Moreover, by detuning the excitation to 760 nm, the reversal of the radiation direction can be achieved with comparable radiated power, sacrificing only slightly the side lobe level in both directions. Therefore, this result not only provides a design for tunable radiation directionality at the same wavelength but also demonstrates that the remarkable directional radiation does not require the control of interparticle distance with subnanometric accuracy.

An alternative solution of directionality reversal is to fix the geometry while changing the operating wavelength, which can be employed for directional color routing.[12,13] We demonstrate this with the backward-radiation configuration ($h = 4$ nm), as shown in Figure 6b. Compared with the previous results at 780 nm wavelength (see Figure 4e), the main lobe of the radiation pattern at 660 nm is along the positive x-axis with even larger amplitude. Such an increase agrees with the green curve in Figure 4a, where the 660 nm wavelength indeed corresponds to greater radiated power.

In addition to the high directionality, metallic nanoantennas also offer the opportunity to greatly enhance the local density of photonic states (LDPS). When a nanoemitter is positioned in an environment with large LDPS, its spontaneous decay rate

DOI: 10.1021/acsphotonics.5b00697
ACS Photonics 2016, 3, 953−963

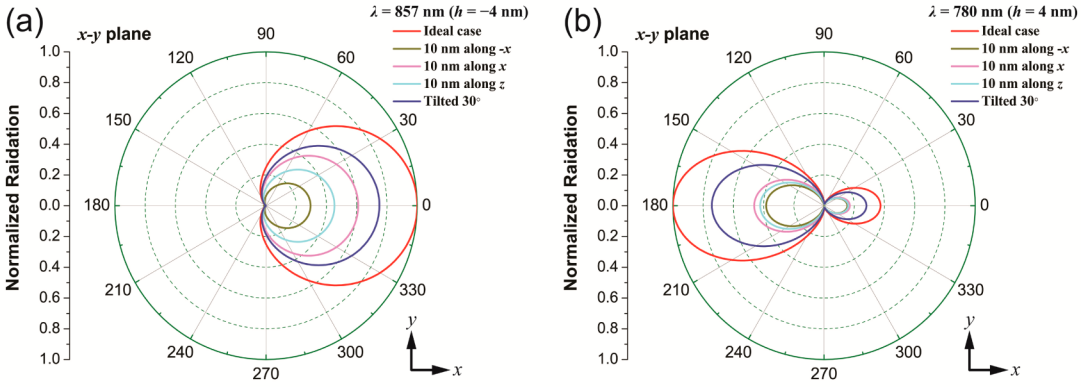

Figure 8. Comparison of radiation patterns under different excitation conditions. The main lobe amplitude is normalized to the value obtained from a perfectly positioned ED emitter (red curves). In nonideal cases, the emitter is either shifted inward (along the $-x$-axis), outward (along the x-axis), or sideways (along the $\pm z$-axis) for 10 nm or tilted 30° with respect to the y-axis. (a) Forward radiation at 857 nm wavelength with $h = -4$ nm (cf. Figure 2e). (b) Backward radiation at 780 nm wavelength with $h = 4$ nm (cf. Figure 4e).

γ can be sustainably enhanced. Such an enhancement is characterized by the Purcell factor F_p,[56−58] which can be calculated by taking the ratio of the emitted power from the emitter with and without plasmonic nanostructures:

$$F_p = \frac{\gamma}{\gamma_0} = \frac{P_{em}}{P_0} = \frac{P_r + P_{nr}}{P_0} \tag{3}$$

Here, γ is the spontaneous emission rate, P_r and P_{nr} account for the radiative and nonradiative part of the total emitted power, respectively, while the subscript "0" indicates the corresponding quantities in the absence of any structures. For the present trimer nanoantenna, the total emission P_{em} can be obtained by integrating the outgoing power flow over a small spherical surface enclosing the nanoemitter only. The denominator, P_0, is available from the classical formula[45,58]

$$P_0 = \frac{c^2 Z k^4}{12\pi} |\vec{p}_0|^2 \tag{4}$$

where $\vec{p}_0$ is the ED vector of the emitter. Figure 7a shows the calculated Purcell factor of the forward-radiation configuration with the red curve, where two distinct peaks appear at 510 and 835 nm. The first peak at 510 nm, giving a 16 000-fold improvement on the spontaneous emission, is related to the interband transition of gold rather than any plasmonic resonant modes.[59] At this spectral region, the photon energy from the emitter mainly dissipates as heat via the nonradiative decay channel and cannot reach the far-field. The presence of the second peak around 835 nm, with the Purcell enhancement of about 8000, is caused by the resonant modes excited in the trimer. Also shown in Figure 7a is the spectrum of the radiation enhancement (blue curve), which is mapped from the radiation spectrum in Figure 2a by normalizing the power as $f = P_r/P_0$. Due to the good radiation capability of the nanoantenna, the resultant quantum yield (green curve), defined as $\eta = P_r/P_{em}$ or simply expressed as $\eta = f/F_p$, is fairly high over the wavelength range between the resonances, exceeding 0.6 in contrast to the near-zero value at short wavelengths. Thus, a larger portion of the emitted power from the emitter is coupled to the radiative channel at plasmonic resonances. The spectra of the backward-radiation configuration are presented in Figure 7b. All the features on the short wavelength side are almost unaltered, confirming their origin from the material rather than structures. On the other hand, the peak that accords with plasmonic modes shifts correspondingly to around 720 nm in the Purcell factor and radiation enhancement spectra. These results clearly demonstrate that our nanoantennas can provide remarkable emission enhancement in addition to the tunable radiation directionality.

In practice, neither the position nor the orientation of the dipole emitter can be perfectly controlled. However, the recent advances in DNA origami and self-assembly have shown the potential to position nanoparticles with extremely high precision. In the case where the emitter is bound to the dimer gap by DNA staples, the shortest stapling strands measuring about 18 base-pairs long (~6 nm) will confine the emitter to a very small volume around the desired site.[60,61] Figure 8 reports the normalized radiation patterns of the forward ($h = -4$ nm) and backward ($h = 4$ nm) radiation configuration with nonideal excitations. When the exciting dipole is shifted along the x-, $-x$-, and z-axis for 10 nm, in all cases the directionality is well preserved despite a decrease in the radiated power. This decrease is because a dislocation of the source from the hot spot of gap-plasmons reduces both the decay rate enhancement and photon-radiation efficiency.[62,63] We also find that when the exciting dipole is polarized perpendicular to the dimer's orientation, i.e., along the x- or z-axis, none of the aforementioned plasmonic modes can be effectively excited and the radiated power is 3 to 4 orders of magnitude weaker (not shown) than the value from the desired arrangement. This is consistent with previous work.[57,60] Consequently, for a tilted emitter, only the component projected in the y direction is useful in boosting the radiation. The radiated power is thus proportional to the square of this component. Figure 8 also shows the radiation pattern of a dipole at the gap center but tilted 30° about the y-axis. The normalized main lobe amplitude equals 0.75, agreeing well with the prediction based on the angular projection. In sensing applications, the nanoparticles and target molecules are both dispersed in solution. Under illumination, only the molecules residing in the vicinity of the gaps and polarized along the correct orientation will be excited efficiently. Nevertheless, as demonstrated above, near the resonance their coupling to the nanoantennas yields roughly a 4000-fold enhancement of the radiated power. Therefore, the detection sensitivity can still be enhanced enormously, even though only a small portion of the target molecules are located in the vicinity of the gaps.[64]

DOI: 10.1021/acsphotonics.5b00697
ACS Photonics 2016, 3, 953−963

In conclusion, we have designed and numerically demonstrated an ultracompact nanoantenna with tunable directionality of radiation. The nanoantenna, which consists of three plasmonic nanoparticles assembled in a symmetry-broken trimer configuration, can support a highly tunable magnetic resonance when the third, larger particle is placed in close proximity to the two smaller particles. The MD interferes with the ED mode under conditions close to those of the Kerker scattering, giving rise to superior forward radiation with a side lobe level as low as −22 dB and a considerable −10 dB bandwidth of 50 nm. The reversal of radiation direction is accomplished by moving the larger particle a few nanometers away from the dimer, whereby the side lobe level of the backward radiation retains the peak value of −4.2 dB within a bandwidth of ∼10 nm. The designs are further optimized so that the reversal of radiation direction can be achieved at the same wavelength. The radiation patterns for both forward and backward radiation are well reproduced with analytic formulas based on a simple dipole model. Furthermore, quantitative calculations show that the Purcell factor and radiated power are enhanced by 4 and 3 orders of magnitude, respectively, manifesting a possible avenue to ultrafast and ultrabright light sources.

The recent progress in DNA-assisted metamaterials,[40] reconfigurable metamolecules,[41] and "plasmonic walkers"[65] has demonstrated that the configuration of nanoparticle clusters can be actively controlled with a nanometric precision. The dimension of the particles, gaps, and movement in our design falls potentially into the applicable range of this technique. We thus believe the experimental demonstration of the proposed nanoantenna is feasible and foresee that applications including chemo-/biosensing, directional emitters, couplers and sorters will benefit from our designs.[12] In addition, the nanoparticle cluster can be transformed in different ways to fit various practical demands. For instance, scaling the particle sizes can shift the desired performance to different operating wavelengths, and replacing spherical nanoparticles with nanodisks makes the device compatible with on-chip photonic circuits.[33] Furthermore, magnetic resonance exists not only in plasmonic trimers but also in other building blocks such as SRRs,[66] nanodisk pairs,[10,67] diabolo nanoantennas,[68] and high-index dielectric particles.[23−25] Even naturally existing materials, such as lanthanide ions, can provide strong MD transitions at optical frequencies.[69] A further study on magnetic resonance in these systems and the relevant light−matter interactions will show their true colors in more applications.

METHODS

Finite Integration Technique Modeling. Simulations were performed using CST Microwave Studio 2014. Frequency domain solver was adopted for better accuracy. The ED emitter was modeled using a discrete port mimicking a constant current segment (2.5 mA in a wire of length 0.4 nm). In order to well resolve the strong local fields within the tiny interparticle gaps, dummy spheres were added in the gaps (filled with the background medium $n = 1.33$), and local meshes were activated there. For example, a maximum step width of 1 nm was used for the sphere in the dimer gap. The setting of this parameter varied for different gap sizes between the larger particle and smaller particles. The open boundaries were selected as default (standard impedance boundary condition) with additional space before mesh generation. Depending on the symmetry properties of the system (here mainly determined by the port's position and orientation), proper symmetry plane(s) can be used to save memory and reduce the simulation time.

Finite Element Method Modeling. Simulations were performed using COMSOL 4.3b RF module. The ED emitter was modeled as an electric current dipole moment. The amplitude (10^{-12} A·m) and orientation of a constant current segment were assigned to a single point at the dimer gap center. Dummy spheres were also used in the gaps with very fine meshes. To calculate the Purcell factor, an additional 1 nm dummy sphere enclosing the point dipole was added, discretized with extremely fine meshes with a maximum size of 0.1 nm or smaller. The simulation domain was at least one wavelength in radius and was surrounded by a spherical shell of perfectly matched layer (PML). The outermost boundary was assigned a scattering boundary condition to minimize possible reflection. Far-field calculations were performed on a sufficiently large spherical surface (nearly touching the PML) to ensure the accuracy of the near-field to far-field transformation. Two probes were set 1 m away from the origin on the *y*- and *z*-axis, respectively. Test runs with different mesh sizes and domain sizes were conducted until convergence was reached.

The surface charge density plots were obtained by applying Gauss's law to the local fields at the metal/dielectric interfaces. Specifically, the charge distribution was calculated by taking the difference between the normal component of the electric field closely outside and inside each particle's interface.

ASSOCIATED CONTENT

Supporting Information

The Supporting Information is available free of charge on the ACS Publications website at DOI: 10.1021/acsphotonics.5b00697.

Near-field distribution of the higher order mode; evolution of directionality from the trimer configurations studied in Figure 3 (PDF)

AUTHOR INFORMATION

Corresponding Author

*E-mail: y.liu@neu.edu.

Notes

The authors declare no competing financial interest.

ACKNOWLEDGMENTS

The authors acknowledge the financial support from the Office of Naval Research under award number N00014-16-1-2049.

REFERENCES

(1) Novotny, L.; Van Hulst, N. Antennas for light. *Nat. Photonics* **2011**, *5*, 83−90.
(2) Rotenberg, N.; Kuipers, L. Mapping nanoscale light fields. *Nat. Photonics* **2014**, *8*, 919−926.
(3) Ahmed, A.; Gordon, R. Single molecule directivity enhanced Raman scattering using nanoantennas. *Nano Lett.* **2012**, *12*, 2625−2630.
(4) Atwater, H. A.; Polman, A. Plasmonics for improved photovoltaic devices. *Nat. Mater.* **2010**, *9*, 205−213.
(5) Kinkhabwala, A.; Yu, Z.; Fan, S.; Avlasevich, Y.; Müllen, K.; Moerner, W. Large single-molecule fluorescence enhancements produced by a bowtie nanoantenna. *Nat. Photonics* **2009**, *3*, 654−657.
(6) Chen, P.-Y.; Argyropoulos, C.; Alù, A. Enhanced nonlinearities using plasmonic nanoantennas. *Nanophotonics* **2012**, *1*, 221−233.

DOI: 10.1021/acsphotonics.5b00697
ACS Photonics 2016, 3, 953−963

(7) Aouani, H.; Navarro-Cia, M.; Rahmani, M.; Sidiropoulos, T. P.; Hong, M.; Oulton, R. F.; Maier, S. A. Multiresonant broadband optical antennas as efficient tunable nanosources of second harmonic light. *Nano Lett.* **2012**, *12*, 4997−5002.
(8) Pakizeh, T.; Käll, M. Unidirectional ultracompact optical nanoantennas. *Nano Lett.* **2009**, *9*, 2343−2349.
(9) Kosako, T.; Kadoya, Y.; Hofmann, H. F. Directional control of light by a nano-optical Yagi-Uda antenna. *Nat. Photonics* **2010**, *4*, 312−315.
(10) Liu, Y.; Palomba, S.; Park, Y.; Zentgraf, T.; Yin, X.; Zhang, X. Compact magnetic antennas for directional excitation of surface plasmons. *Nano Lett.* **2012**, *12*, 4853−4858.
(11) Bonod, N.; Devilez, A.; Rolly, B.; Bidault, S.; Stout, B. Ultracompact and unidirectional metallic antennas. *Phys. Rev. B: Condens. Matter Mater. Phys.* **2010**, *82*, 115429.
(12) Shegai, T.; Chen, S.; Miljković, V. D.; Zengin, G.; Johansson, P.; Käll, M. A bimetallic nanoantenna for directional colour routing. *Nat. Commun.* **2011**, *2*, 481.
(13) Alavi Lavasani, S.; Pakizeh, T. Color-switched directional ultracompact optical nanoantennas. *J. Opt. Soc. Am. B* **2012**, *29*, 1361−1366.
(14) Hancu, I. M.; Curto, A. G.; Castro-López, M.; Kuttge, M.; van Hulst, N. F. Multipolar interference for directed light emission. *Nano Lett.* **2013**, *14*, 166−171.
(15) Vercruysse, D.; Zheng, X.; Sonnefraud, Y.; Verellen, N.; Di Martino, G.; Lagae, L.; Vandenbosch, G. A.; Moshchalkov, V. V.; Maier, S. A.; Van Dorpe, P. Directional fluorescence emission by individual V-antennas explained by mode expansion. *ACS Nano* **2014**, *8*, 8232−8241.
(16) Curto, A. G.; Volpe, G.; Taminiau, T. H.; Kreuzer, M. P.; Quidant, R.; van Hulst, N. F. Unidirectional emission of a quantum dot coupled to a nanoantenna. *Science* **2010**, *329*, 930−933.
(17) Maksymov, I. S.; Staude, I.; Miroshnichenko, A. E.; Kivshar, Y. S. Optical yagi-uda nanoantennas. *Nanophotonics* **2012**, *1*, 65−81.
(18) Dregely, D.; Taubert, R.; Dorfmüller, J.; Vogelgesang, R.; Kern, K.; Giessen, H. 3D optical Yagi-Uda nanoantenna array. *Nat. Commun.* **2011**, *2*, 267.
(19) Kim, J.; Roh, Y.-G.; Cheon, S.; Choe, J.-H.; Lee, J.; Lee, J.; Jeong, H.; Kim, U. J.; Park, Y.; Song, I. Y. Babinet-inverted optical Yagi-Uda antenna for unidirectional radiation to free space. *Nano Lett.* **2014**, *14*, 3072−3078.
(20) Kruk, S. S.; Decker, M.; Staude, I.; Schlecht, S.; Greppmair, M.; Neshev, D. N.; Kivshar, Y. S. Spin-polarized photon emission by resonant multipolar nanoantennas. *ACS Photonics* **2014**, *1*, 1218−1223.
(21) Luk'yanchuk, B.; Zheludev, N. I.; Maier, S. A.; Halas, N. J.; Nordlander, P.; Giessen, H.; Chong, C. T. The Fano resonance in plasmonic nanostructures and metamaterials. *Nat. Mater.* **2010**, *9*, 707−715.
(22) Vercruysse, D.; Sonnefraud, Y.; Verellen, N.; Fuchs, F. B.; Di Martino, G.; Lagae, L.; Moshchalkov, V. V.; Maier, S. A.; Van Dorpe, P. Unidirectional side scattering of light by a single-element nanoantenna. *Nano Lett.* **2013**, *13*, 3843−3849.
(23) Geffrin, J.-M.; García-Cámara, B.; Gómez-Medina, R.; Albella, P.; Froufe-Pérez, L.; Eyraud, C.; Litman, A.; Vaillon, R.; González, F.; Nieto-Vesperinas, M. Magnetic and electric coherence in forward-and back-scattered electromagnetic waves by a single dielectric sub-wavelength sphere. *Nat. Commun.* **2012**, *3*, 1171.
(24) Evlyukhin, A. B.; Novikov, S. M.; Zywietz, U.; Eriksen, R. L.; Reinhardt, C.; Bozhevolnyi, S. I.; Chichkov, B. N. Demonstration of magnetic dipole resonances of dielectric nanospheres in the visible region. *Nano Lett.* **2012**, *12*, 3749−3755.
(25) Fu, Y. H.; Kuznetsov, A. I.; Miroshnichenko, A. E.; Yu, Y. F.; Luk'yanchuk, B. Directional visible light scattering by silicon nanoparticles. *Nat. Commun.* **2013**, *4*, 1527.
(26) Liu, W.; Miroshnichenko, A. E.; Neshev, D. N.; Kivshar, Y. S. Broadband unidirectional scattering by magneto-electric core-shell nanoparticles. *ACS Nano* **2012**, *6*, 5489−5497.
(27) Krasnok, A. E.; Simovski, C. R.; Belov, P. A.; Kivshar, Y. S. Superdirective dielectric nanoantennas. *Nanoscale* **2014**, *6*, 7354−7361.
(28) Devilez, A.; Stout, B.; Bonod, N. Compact metallo-dielectric optical antenna for ultra directional and enhanced radiative emission. *ACS Nano* **2010**, *4*, 3390−3396.
(29) Husnik, M.; Klein, M. W.; Feth, N.; König, M.; Niegemann, J.; Busch, K.; Linden, S.; Wegener, M. Absolute extinction cross-section of individual magnetic split-ring resonators. *Nat. Photonics* **2008**, *2*, 614−617.
(30) Fan, J. A.; Wu, C.; Bao, K.; Bao, J.; Bardhan, R.; Halas, N. J.; Manoharan, V. N.; Nordlander, P.; Shvets, G.; Capasso, F. Self-assembled plasmonic nanoparticle clusters. *Science* **2010**, *328*, 1135−1138.
(31) Sheikholeslami, S. N.; Garcia-Etxarri, A.; Dionne, J. A. Controlling the interplay of electric and magnetic modes via Fano-like plasmon resonances. *Nano Lett.* **2011**, *11*, 3927−34.
(32) Shafiei, F.; Monticone, F.; Le, K. Q.; Liu, X.-X.; Hartsfield, T.; Alù, A.; Li, X. A subwavelength plasmonic metamolecule exhibiting magnetic-based optical Fano resonance. *Nat. Nanotechnol.* **2013**, *8*, 95−99.
(33) Nazir, A.; Panaro, S.; Proietti Zaccaria, R.; Liberale, C.; De Angelis, F.; Toma, A. Fano coil-type resonance for magnetic hot-spot generation. *Nano Lett.* **2014**, *14*, 3166−3171.
(34) Hopkins, B.; Poddubny, A. N.; Miroshnichenko, A. E.; Kivshar, Y. S. Revisiting the physics of Fano resonances for nanoparticle oligomers. *Phys. Rev. A: At., Mol., Opt. Phys.* **2013**, *88*, 053819.
(35) Sheikholeslami, S. N.; Alaeian, H.; Koh, A. L.; Dionne, J. A. A metafluid exhibiting strong optical magnetism. *Nano Lett.* **2013**, *13*, 4137−4141.
(36) Chuntonov, L.; Haran, G. Trimeric plasmonic molecules: the role of symmetry. *Nano Lett.* **2011**, *11*, 2440−2445.
(37) Lu, G.; Wang, Y.; Chou, R. Y.; Shen, H.; He, Y.; Cheng, Y.; Gong, Q. Directional side scattering of light by a single plasmonic trimer. *Laser Photonics Rev.* **2015**, *9*, 530−537.
(38) Shegai, T.; Li, Z.; Dadosh, T.; Zhang, Z.; Xu, H.; Haran, G. Managing light polarization via plasmon−molecule interactions within an asymmetric metal nanoparticle trimer. *Proc. Natl. Acad. Sci. U. S. A.* **2008**, *105*, 16448−16453.
(39) Johnson, P. B.; Christy, R.-W. Optical constants of the noble metals. *Phys. Rev. B* **1972**, *6*, 4370.
(40) Kuzyk, A.; Schreiber, R.; Fan, Z.; Pardatscher, G.; Roller, E.-M.; Högele, A.; Simmel, F. C.; Govorov, A. O.; Liedl, T. DNA-based self-assembly of chiral plasmonic nanostructures with tailored optical response. *Nature* **2012**, *483*, 311−314.
(41) Kuzyk, A.; Schreiber, R.; Zhang, H.; Govorov, A. O.; Liedl, T.; Liu, N. Reconfigurable 3D plasmonic metamolecules. *Nat. Mater.* **2014**, *13*, 862−866.
(42) Roller, E.-M.; Khorashad, L. K.; Fedoruk, M.; Schreiber, R.; Govorov, A. O.; Liedl, T. DNA-assembled nanoparticle rings exhibit electric and magnetic resonances at visible frequencies. *Nano Lett.* **2015**, *15*, 1368−1373.
(43) Prodan, E.; Radloff, C.; Halas, N. J.; Nordlander, P. A hybridization model for the plasmon response of complex nanostructures. *Science* **2003**, *302*, 419−422.
(44) Arango, F. B.; Koenderink, A. F. Polarizability tensor retrieval for magnetic and plasmonic antenna design. *New J. Phys.* **2013**, *15*, 073023.
(45) Jackson, J. D. *Classical Electrodynamics*, third ed.; Wiley, 1999.
(46) Sauvan, C.; Hugonin, J. P.; Maksymov, I. S.; Lalanne, P. Theory of the spontaneous optical emission of nanosize photonic and plasmon resonators. *Phys. Rev. Lett.* **2013**, *110*, 237401.
(47) Yang, J.; Perrin, M.; Lalanne, P. Analytical formalism for the interaction of two-level quantum systems with metal nanoresonators. *Phys. Rev. X* **2015**, *5*, 021008.
(48) Kerker, M.; Wang, D.-S.; Giles, C. Electromagnetic scattering by magnetic spheres. *J. Opt. Soc. Am.* **1983**, *73*, 765−767.
(49) Balanis, C. A. *Antenna Theory: Analysis and Design*, third ed.; John Wiley & Sons, 2012.

DOI: 10.1021/acsphotonics.5b00697
ACS Photonics 2016, 3, 953−963

(50) Rotenberg, N.; Krijger, T.; le Feber, B.; Spasenović, M.; de Abajo, F. J. G.; Kuipers, L. Magnetic and electric response of single subwavelength holes. *Phys. Rev. B: Condens. Matter Mater. Phys.* **2013**, *88*, 241408.
(51) Rodríguez-Fortuño, F. J.; Marino, G.; Ginzburg, P.; O'Connor, D.; Martínez, A.; Wurtz, G. A.; Zayats, A. V. Near-field interference for the unidirectional excitation of electromagnetic guided modes. *Science* **2013**, *340*, 328−330.
(52) Mueller, J. B.; Capasso, F. Asymmetric surface plasmon polariton emission by a dipole emitter near a metal surface. *Phys. Rev. B: Condens. Matter Mater. Phys.* **2013**, *88*, 121410.
(53) Cho, D. J.; Wang, F.; Zhang, X.; Shen, Y. R. Contribution of the electric quadrupole resonance in optical metamaterials. *Phys. Rev. B: Condens. Matter Mater. Phys.* **2008**, *78*, 121101.
(54) Petschulat, J.; Yang, J.; Menzel, C.; Rockstuhl, C.; Chipouline, A.; Lalanne, P.; Tünnermann, A.; Lederer, F.; Pertsch, T. Understanding the electric and magnetic response of isolated metaatoms by means of a multipolar field decomposition. *Opt. Express* **2010**, *18*, 14454−14466.
(55) Rolly, B.; Stout, B.; Bidault, S.; Bonod, N. Crucial role of the emitter−particle distance on the directivity of optical antennas. *Opt. Lett.* **2011**, *36*, 3368−3370.
(56) Purcell, E. M. Spontaneous emission probabilities at radio frequencies. *Phys. Rev.* **1946**, *69*, 681.
(57) Cang, H.; Liu, Y.; Wang, Y.; Yin, X.; Zhang, X. Giant suppression of photobleaching for single molecule detection via the Purcell effect. *Nano Lett.* **2013**, *13*, 5949−5953.
(58) Novotny, L.; Hecht, B. *Principles of Nano-Optics*, second ed.; Cambridge University Press, 2012.
(59) Corti, C.; Holliday, R. *Gold: Science and Applications*; CRC Press, 2009.
(60) Acuna, G.; Möller, F.; Holzmeister, P.; Beater, S.; Lalkens, B.; Tinnefeld, P. Fluorescence enhancement at docking sites of DNA-directed self-assembled nanoantennas. *Science* **2012**, *338*, 506−510.
(61) Pellegrotti, J. V.; Acuna, G. P.; Puchkova, A.; Holzmeister, P.; Gietl, A.; Lalkens, B.; Stefani, F. D.; Tinnefeld, P. Controlled reduction of photobleaching in DNA origami−gold nanoparticle hybrids. *Nano Lett.* **2014**, *14*, 2831−2836.
(62) Akselrod, G. M.; Argyropoulos, C.; Hoang, T. B.; Ciracì, C.; Fang, C.; Huang, J.; Smith, D. R.; Mikkelsen, M. H. Probing the mechanisms of large Purcell enhancement in plasmonic nanoantennas. *Nat. Photonics* **2014**, *8*, 835−840.
(63) Faggiani, R.; Yang, J.; Lalanne, P. Quenching, plasmonic, and radiative decays in nanogap emitting devices. *ACS Photonics* **2015**, *2*, 1739−1744.
(64) Punj, D.; Regmi, R.; Devilez, A.; Plauchu, R.; Moparthi, S. B.; Stout, B.; Bonod, N.; Rigneault, H.; Wenger, J. Self-assembled nanoparticle dimer antennas for plasmonic-enhanced single-molecule fluorescence detection at micromolar concentrations. *ACS Photonics* **2015**, *2*, 1099−1107.
(65) Zhou, C.; Duan, X.; Liu, N. A plasmonic nanorod that walks on DNA origami. *Nat. Commun.* **2015**, *6*, 8102.
(66) Hein, S. M.; Giessen, H. Tailoring magnetic dipole emission with plasmonic split-ring resonators. *Phys. Rev. Lett.* **2013**, *111*, 026803.
(67) Feng, T.; Zhou, Y.; Liu, D.; Li, J. Controlling magnetic dipole transition with magnetic plasmonic structures. *Opt. Lett.* **2011**, *36*, 2369−2371.
(68) Grosjean, T.; Mivelle, M.; Baida, F.; Burr, G.; Fischer, U. Diabolo nanoantenna for enhancing and confining the magnetic optical field. *Nano Lett.* **2011**, *11*, 1009−1013.
(69) Taminiau, T. H.; Karaveli, S.; van Hulst, N. F.; Zia, R. Quantifying the magnetic nature of light emission. *Nat. Commun.* **2012**, *3*, 979.

DOI: 10.1021/acsphotonics.5b00697
ACS Photonics 2016, 3, 953−963